A Numerical Exploration of Engine Combustion Using Toluene Reference Fuel and Hydrogen Mixtures

Alessio Barbato[1,*], *Valentina* Pessina[1], *Massimo* Borghi[1]

[1]Department of Engineering "Enzo Ferrari", University of Modena and Reggio Emilia, Modena 41125, Italy

Abstract. Hydrogen-fueled internal combustion engines (H2ICEs) are capable of operating over a wide range of equivalence ratios: from ultra-lean mode to stoichiometric conditions. However, they provide maximum thermal efficiency and minimum NOx emissions if operated lean. Although NOx is produced, H2ICEs generate little or no CO, CO2, SO2, HC, or PM emissions. The main limitation to pure hydrogen fueling is power density. To overcome such an issue, mixtures of gasoline and hydrogen can be exploited, with small modifications to the engine feeding system. Due to the peculiar characteristics of hydrogen (in terms of thermophysical properties, molecular weight and propagating flame characteristics) care must be adopted when trying to address combustion using computational fluid dynamics (CFD) tools. In this work, we simulate the combustion of mixtures of toluene reference fuel (TRF) and hydrogen under largely different ratios. To simplify the problem, liquid and gaseous injections are neglected, and a premixed mixture at the inlet of the CFD domain is imposed. Due to the different laminar flame speeds of the mixture components, mass-fraction weighted in-house correlations based on chemical kinetics simulations are adopted. Outcomes are compared with those obtained using standard correlations and mixing rules available in most commercial CFD packages.

1 Introduction

The European Green Deal [1] sets out the European Union's (EU) path to climate neutrality by 2050, through the deep decarbonization of all sectors of the economy; anthropogenic greenhouse gas (GHG) emission reductions are also set for 2030. This is not the first compact of the EU Commission aiming at the reduction of GHG emissions. Back in 2009, the EU imposed very challenging targets to strictly reduce GHG emissions with the Renewable Energy Directive [2] (RED). According to the European Parliament and Council [3], road transport accounted for 22% of the EU GHG emissions in 2015. For this reason, a Revised Renewable Energy Directive (REDII) [4] imposed that at least 10% of

* Corresponding author: alessio.barbato@unimore.it

the energy used in transportation must be bio-based by 2020, and the overall EU target for Renewable Energy Sources consumption by 2030 has been raised to 32%. The Commission's original proposal did not include a transport sub-target, which has been introduced by co-legislators in the final agreement: all Member States must require fuel suppliers to supply at least 14% of the energy consumed in road and rail transport by 2030 as renewable energy. Thus, in the last few years, biofuels have increasingly gained the attention of researchers in the automotive industry as a doable solution to cleaner powertrains, in compliance with EU regulations. Ethanol is the main biofuel currently used in production engines: besides being a renewable source of energy, it also has lower production costs compared to other alcohols, such as methanol or n-butanol [5, 6]. Several experimental studies investigated the pure bio-alcohol fuels combustion characteristics in modern direct-injection spark-ignition engines (DISI). Irimescu et al. [7] compared stoichiometric butanol and ethanol mixtures in terms of combustion indicators and emissions in an optically accessible DISI research engine operated at full load. As shown by Di Iorio et al. [8], the addition of ethanol increases the octane number of the fuel, thus allowing an increase of the spark advances and/or a higher compression ratio. However, Sarathy et al. [9] highlighted that the addition of oxygenates led to a reduction of the mass-based Lower Heating Value (LHV) of the fuel blend because fuel-oxygen atoms do not contribute to heat production; therefore, the reduction of the LHV is proportional to the mass percentage of oxygen. Hydrogen (H2) can be considered as a brighter fuel/additive to reduce internal combustion engines' (ICEs) emissions. As a matter of fact, H2ICEs have near-zero emissions levels and efficiencies higher than modern ICEs [10]. Furthermore, the well-to-wheel GHG reduction of H2ICE vehicles compared to hydrocarbon-fueled ones turns out to be positive [11]. H2 seems to be a feasible solution for current/future transportation, and H2ICEs could act as a bridging technology towards a widespread H2 infrastructure for alternative propulsion technologies such as fuel cells [12-14] since H2ICE vehicles can be operated also with conventional fuel.

The peculiar properties of H2 compared to both conventional liquid/gaseous fuels, such as gasoline and methane, make it a promising fuel for ICE applications, despite its low minimum ignition energy of 0.02 mJ requires caution when using it as an engine fuel. Its laminar flame speed, at stoichiometric conditions, is approximately 5 times faster than the one of gasoline or methane. As the wide flammability limits ranging from 4 to 75 vol% of H2 in air allow H2ICEs to be operated with substantial dilution (excess air or EGR), laminar flame speed and flame stability can vary largely, and consequently are important parameters that must be considered. The same properties that make H2 such a fascinating fuel for ICEs also account for peculiar combustion events. The wide flammability limits together with the low ignition energy required and the high flame speeds could lead to undesired combustion phenomena such as autoignition and backfiring. The latter is limited to port fuel injection (PFI) operation and can be avoided with DI operation, as adopted in the modern H2ICEs. The correlation between mixture quality and NOx – the only relevant emission component in H2ICEs - is well documented in the literature. At fuel-to-air equivalence ratios (ϕ) of less than 0.5 ($\lambda > 2$), the engine operates without generating NOx emissions; increasing ϕ beyond this threshold results in an increase of NOx emissions peaking around $\phi \sim 0.75$ and a slight decrease approaching stoichiometric mixtures. It has been demonstrated [15] that the use of a multiple injection strategy in H2-DI ICEs is an effective measure to significantly reduce NOx emissions, up to 95%. Further emission reduction could be gained including EGR and water injection as well as aftertreatment concepts like 3-way catalysts as well as lean NOx traps. The emission levels of modern H2ICE vehicles are by far within the most severe standards while overcoming the fuel economy of their conventional-fuel counterparts. Aside from the use as a neat fuel, H2 is also considered as a combustion enhancer and blending agent with gaseous fuels or in bi-

fuel operated ICEs, with both gasoline and diesel-like fuels. A 15% increase of power/density in H2-doped DI ICEs compared to gasoline-fueled units has also been demonstrated [16], and extrapolations from single-cylinder engine efficiency data suggest that a brake thermal efficiency of 45% is achievable. In the design and optimization of H2-doped ICEs, 3D-CFD can be a very promising tool given its ability to span a wide range of technical solutions with reduced times and costs. In the simulation of the combustion phenomena in spark-ignition (SI) engines, flamelet combustion models are largely used by the user community. Despite several flamelet models are available, all of them require laminar flame speed (LFS) as an input to properly estimate the turbulent burn rate. In this work, a TRF surrogate mixed with H2 is used, suitable for representing gasoline-hydrogen blends up to 95%mol of hydrogen. LFS of the blend is provided as an input using a linear mixing rule of the laminar velocity of the two components. In this study, an H2 LFS correlation is derived at typical full-load conditions of GDI engines based on chemical kinetics simulation results, carried out in DARSv4.30 licensed by Siemens DISW, and the reaction mechanisms developed by [17, 18]. Then, using the aforementioned linear mixing rule, it is combined with a TRF LFS correlation previously developed by the authors in [19-21]. Results are implemented in a 3D-CFD software to correctly reproduce the different combustion phenomena based on the mole fraction of H2 in the blend. The outcomes show how the addition of H2 in conventional-fuels ICEs leads to a higher power ratio with low emissions and higher fuel economy.

2 3D-CFD Domain

A simplified engine geometry, yet fully representative of currently made DISI units, is adopted in this study. The engine is based on a Ford Motor Company unit, simplified to gain stability and to reduce the complexity of the 3D model. It is a 4-valves pent-roof engine featuring a wall-guided gasoline direct injection system. A Detailed list of engine specifications and operating point is reported in Table 1.

Table 1 - Detailed Engine Specifications

Parameter	Specification
Displacement Volume	402.0 cc
Bore	80 mm
Stroke	80 mm
Connecting Rod Length	139.0 mm
Compression Ratio	9.0:1
Engine Speed	6500 Rpm
Fuel/Air Equivalence Ratio	1.0
Fuel	TRF-H2 blends (0.0, 50.0, 70.0, 95.0%mol of H2)
Intake Pressure	1.80 bar
Intake Temperature	46.85 °C

Constant pressures and temperatures representative of a full-load operation are imposed at the intake inlet and exhaust outlet: a value of 1.8bar is set as inlet pressure at 320K, while a backpressure of 2.0bar and a temperature of 950K is imposed at the exhaust outlet. Fuel injection is replaced by a premixed mixture of air and fuel. Four different H2/TRF blends are tested. The TRF part is a mixture of iso-octane, n-heptane, and toluene purposely formulated to represent a ULG95 “average gasoline”, according to the EN228 specification. The blends differ by the H2 mole fraction they contain, respectively 0%, 30%, 50%, and 95%. Further details can be found in Table 2.

Table 2 - Blend Compositions

Blend	Components	Mole Fraction	Mass Fraction
Pure TRF	H2	0.0000	0.0000
	iso-C8H18	0.4094	0.4571
	C7H16	0.1391	0.1363
	C7H8	0.4515	0.4067
50% H2 – 50% TRF	H2	0.5000	0.0193
	iso-C8H18	0.2047	0.4483
	C7H16	0.0696	0.1336
	C7H8	0.2258	0.3988
70% H2 – 30% TRF	H2	0.7000	0.0440
	iso-C8H18	0.1228	0.4370
	C7H16	0.0417	0.1303
	C7H8	0.1355	0.3888
95% H2 – 5% TRF	H2	0.9500	0.2724
	iso-C8H18	0.0205	0.3326
	C7H16	0.0070	0.0991
	C7H8	0.0226	0.2959

3 Numerical Setup

In this study, a RANS approach to turbulence is adopted for the simulation of the combustion behavior by using the commercial CFD-3D software SimCenter STAR-CCM+ v2021.1 licensed by Siemens DISW. RANS is preferred to other more refined techniques such as DES [22-24] or LES [25-28] since focus is made at present on the average engine performance, without claiming to cover phenomena such as CoV [29], knock [30-32] or misfire [33].

3.1 Computational Grid

The meshing tool uses a cell trimming process coupled with a dedicated prismatic mesher for the near-wall grid. Mesh motion is handled by a morphing / remapping technique. Whenever cell quality drops below user-editable quality metrics, a new mesh is generated and results are conservatively interpolated onto the new grid.

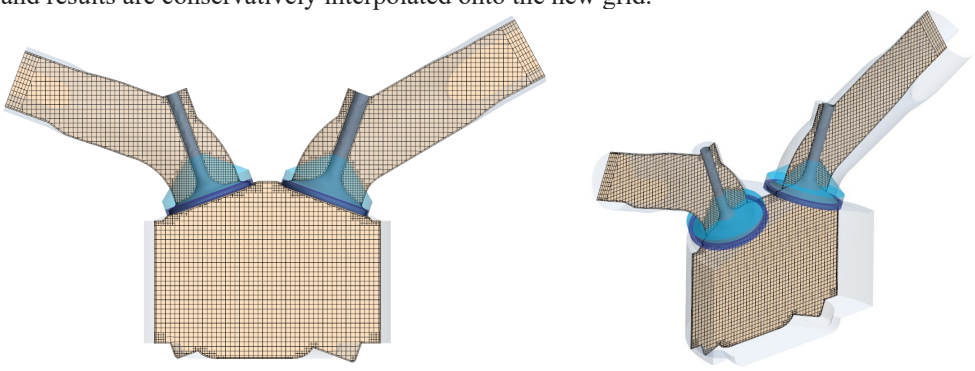

a) b)

Figure 1 - Computational grid onto Y valves section plane, with CVs highlighted in different colors.

The in-cylinder core grid spacing is equal to 1.5mm, with fixed and moving adaptive control volumes (CVs) to reduce local cell size down to 0.375mm. In particular, crank angle-dependent control volumes are activated to handle valve openings and closures. The near-wall grid all over the domain is composed of a single layer with a near-wall thickness

equal to 0.35mm. The mesh, visible in Figure 1, is designed to run multiple setups with limited computational resources. The maximum cell count is around 170.000 cells at bottom dead center (BDC), and 100.000 at top dead center (TDC).

3.2 Physical Models

Time is solved by the PISO algorithm. A monotone advection and reconstruction scheme (MARS) is used for temporal and spatial discretization. Turbulence is modeled using the Renormalization Group (RNG) K-Epsilon in combination with the High-y+ wall treatment model. The Ideal Gas equation of state is employed to compute the density and its derivatives as a function of temperature and pressure. Sutherland's law is used for the Dynamic Viscosity, while the Specific Heat is computed using a Mass-Weighted Mixture method. Wall heat transfer is modelled using the GruMo-UniMORE thermal wall function [34-37]. The ECFM-3Z model is adopted for the simulation of the combustion phenomena, coupled with two different laminar flame speed correlations.

3.2.1 Laminar Flame Speed Correlation: Metghalchi and Keck versus GruMoLFSFit

Modeling flame propagation is essential to provide reliable results. ICEs combustion occurs mostly under the flamelet combustion regime: the reaction zone is localized and turbulence interacts with the flame via corrugation of the reaction zone. Turbulent flames in this regime can be modeled as a thickened flame brush, i.e. the turbulent flame is modeled as a thickened laminar flame. Therefore, an accurate input for LFS is essential. The default laminar flame speed is given by the Metgalchi and Keck correlation as in Eq. 1 [38]:

$$s_{\mathrm{L}} = s_{l0}\left(\frac{T_u}{T_0}\right)^{\alpha} \cdot \left(\frac{p}{p_0}\right)^{\beta} \cdot max[\,1 - U_{lam1}X_{res}\,, exp(U_{lam2}X_{res})\,] \tag{1}$$

where:

- s_{l0} is the reference laminar flame speed;
- α e β are functions of local ϕ, and two different formulations for β are implemented to cover p/p_{ref} below and over p_{transl}, being p_{transl} the normalized transitional pressure value for pressure scaling;
- p is pressure, T is temperature, and the subscripts 0 and u denote reference and unburnt gas properties, respectively;
- X_{res} is the mole fraction of the residual gas.
- U_{lam1} and U_{lam2} are the first and second coefficients for EGR respectively.

The reference laminar speed s_{l0} is a weak function of fuel type and it is fit by a second-order polynomial of the following form, Eq. 2:

$$s_{l0} = B_m + B_2\,(\phi - \phi_m)^2 \tag{2}$$

where coefficients ϕ_m, B_m and B_2 are reported in the literature for methanol, propane, and iso-octane. Metghalchi and Keck claim that their LFS is within 10% of the measured data in the operative range of $0.4 \cdot 10^6 \leq p \leq 5 \cdot 10^6$ Pa, $300 \leq T \leq 700$ K, and $0.8 \leq \phi \leq 1.5$.

Following the rationale in [39, 40], the in-house developed correlation expresses the LFS (s_{L}) as a function of the thermodynamic state and mixture quality (e.g., Φ) as reported in Eq. 3. The fitting coefficients for the H2 LFS are reported in Table 3 along with the reference conditions and range of validity.

$$s_{\mathrm{L}}(\phi) = \sum_{\mathrm{i}=1}^{5} \mathrm{a_i} \cdot \left(\ln(\phi)\right)^{\mathrm{i}} \cdot \left(\frac{T_{\mathrm{u}}}{T_{\mathrm{ref}}}\right)^{\left(\sum_{\mathrm{i}=1}^{5} \mathrm{b_i} \cdot (ln(\phi))^{\mathrm{i}}\right)} \cdot \left(\frac{p}{p_{\mathrm{ref}}}\right)^{\left(\sum_{\mathrm{i}=1}^{5} \mathrm{c_i} \cdot (ln(\phi))^{\mathrm{i}}\right)} \quad (3)$$

Table 3 - Fitting coefficients, reference pressure and temperature, and range of validity laminar flame speed correlation for H2 (Eq. 3).

	FIT COEFFICIENTS				
	$\mathbf{a_i}$	$\mathbf{b_i}$	$\mathbf{c_i}$	**Reference Conditions**	
0	579.410304493307	3.08496586863348	-0.662375482056093	T_{ref}	850 K
1	1126.343332515420	-2.38624134397731	0.740611383386044	p_{ref}	$8{\cdot}10^6$ Pa
2	419.543837792955	-1.72046449606166	1.038324743527740	**Validity Range**	
3	-807.618181133741	-1.05803043959888	0.767945985221820	$0.4 < \Phi < 1.0$	
4	-1086.552792428860	6.76986526585950	-1.403901570518590	$600\ \mathrm{K} < T_{\mathrm{u}} < 1075\ \mathrm{K}$	
5	-435.246230176884	5.11161722589838	-1.575252787580020	$3{\cdot}10^5\ \mathrm{Pa} < p < 1.3 \cdot 10^7\ \mathrm{Pa}$	

The percentage errors for the resulting H2 fitted correlation $s_{\mathrm{L,fit}}$ with respect to the chemical kinetics simulations $s_{\mathrm{L,sim}}$ are reported in Figure over a wide range of pressures at stoichiometric condition. For each pressure level, three temperatures are considered with a shift of ± 100 K from the central value. As for the TRF LFS, the correlation developed in [21] is adopted. It is worth to emphasize that the validity range of the correlation is much larger than the one of the Metghalchi and Keck correlation, i.e. covering states which are easily reached by the operating conditions of current production ICEs.

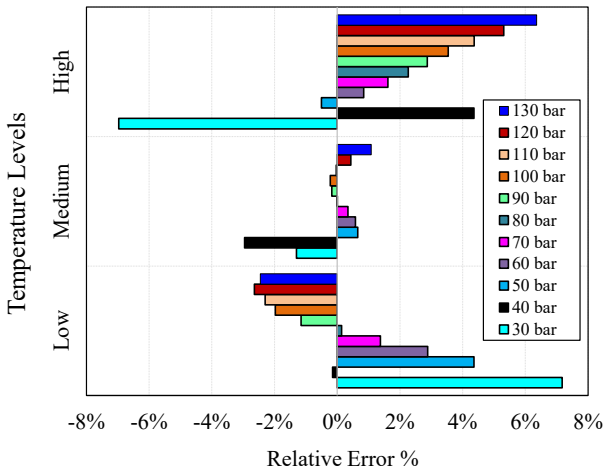

Figure 2 - Relative percentage fitting error (GruMo $s_{l,fit}$ Vs. $s_{l,sim}$) at stoichiometric conditions

Finally, a mixing rule is used to combine the two correlations into the final CFD input. A simple linear by mass fraction rule is used, see Eq. 4:

$$s_{\mathrm{L,BLEND}}(\Phi) = Y_{\mathrm{TRF}}^{\mathrm{BLEND}} \cdot s_{\mathrm{L,TRF}}(\Phi) + Y_{\mathrm{H_2}}^{\mathrm{BLEND}} \cdot s_{\mathrm{L,H_2}}(\Phi) \quad (4)$$

Figure 3 shows a comparison between the Metghalchi and Keck correlation and the GruMo LFS fit for Pure-TRF. Lower LFS values are computed using our in-house correlation,

possibly related to the different conditions in which the fit is validated. Besides the observed differences, it is worth to remark that Metghalchi and Keck correlation is not suitable for H2 combustion, and an alternative correlation to compute the final LFS of the hydrogen-doped fuel should be chosen.

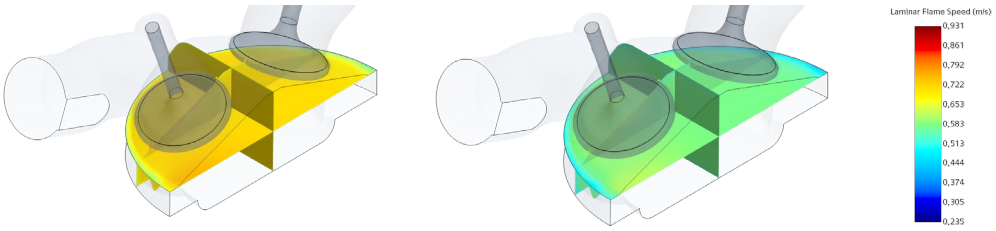

(a) (b)

Figure 3 - Laminar Flame Speed pre-spark (689.0 CA deg), a) Metghalchi & Keck, b) GruMo LFS Fit

A simple energy deposition model is chosen to take care of the ignition process. The simulations share the same combustion model settings. Spark time is set to 690.0 CA deg, for the blend with H2 content equal to 0% mol, while increasing the mole fraction of H2 it is adjusted to achieve reasonably equal phasing of 50% of mass fraction burnt (MFB).

4 Results

A full engine cycle is simulated starting from 80CA degrees After firing TDC (AfTDC). For the sake of brevity, the present analysis focuses on the range from 690CA deg to end of the engine cycle, i.e. 800 CA deg. As a matter of fact, by excluding the fuel injection process, and thus charge cooling due to evaporation and subsequent mixing, differences are limited to changes in the physical properties of the inducted mixture. A first comparison is made between the GruMo LFS correlation and the Metghalchi & Keck correlation in the TRF-only case. Observing the in-cylinder pressure traces and the combustion indicators in Figure 4 a) and b), it is possible to see a slow-down of the first portion of the combustion process using the GruMo LFS correlation, followed by a steeper pressure rise, which in turn leads to a higher pressure peak.

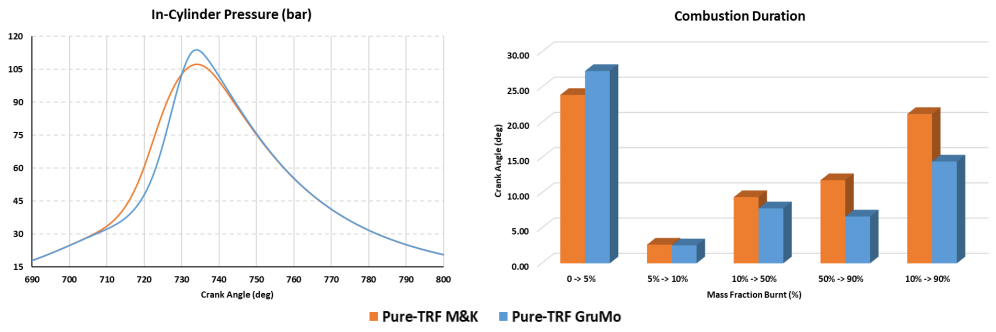

(a) (b)

Figure 4 – In-cylinder pressure traces and combustion phasing of the Pure-TRF simulation with Metghalchi & Keck (Pure-TRF M&K) and GruMo LFS correlation (Pure-TRF GruMo)

An increase in the Indicated Mean Effective Pressure (IMEP) is found by adopting the in-house LFS correlation; values are listed in Table 4.

Table 4 – Metghalchi & Keck vs. GruMo LFS correlation power-output outcomes

	IMEP (bar)	ΔIMEP (%)	Q_{th} (kJ)	Q_{comb} (kJ) (690 -> 790 CAdeg)
Pure TRF M&K	15.999	/	1.1181	1.0761
Pure TRF GruMo	16.150	+ 0.95%	1.1181	1.0795

The introduction of H2 in the inducted fuel on equal inlet conditions, leads to lower energy available in the combustion chamber, Q_{th}, primarily due to the lower density of H2 compared to that of TRF, as shown in Figure 6 b). Figure 5 a) shows the in-cylinder pressure traces resulting by the different tested fuels. A positive trend increasing the H2 content is found in terms of combustion history until a cap is reached: in fact, increasing the H2 content over 70% mol the available Q_{th} is too low to reach the target pressure peak. Looking at Figure 5 b) it is possible to see the phasing of the combustion process. For this set of simulations, the SA of the Pure-TRF is kept at the original value, i.e. 690 CAdeg, while the SA of the others is moved forward to meet nearly equal phasing of 50% of MFB. Increasing the H2 content SA is moved forward by 6.5, 11.5, and 23.4 CAdeg respectively for the 50%, 70% and 95% of H2 content. IMEP is lower than the pure TRF case for all the H2-doped simulations. This is due to the lower Q_{th} in the combustion chamber. However, a remarkable reduction of Brake Specific Fuel Consumption (BSFC) is found for increasing H2 content.

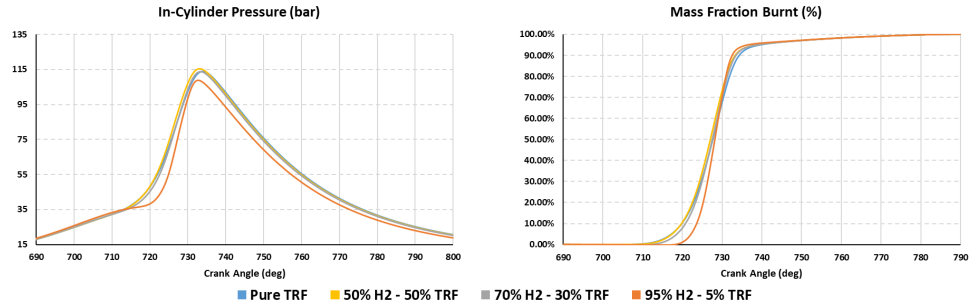

(a) (b)

Figure 5 – In-Cylinder pressure and MFB traces of the different blends, on equal boundary conditions

With a 50% mol of H2 in the fuel, a reduction of Q_{th} equal to 1.05% is found which leads to a reduction of 1.01% of IMEP and a BSFC gain of 3.37%. Moving to 70% mole fraction of H2, the loss in Q_{th} increases to 2.38% with a decrease of IMPE of 2.89% and a gain in BSFC equal to 6.79%. The extreme case of 95% H2 leads to a BSFC saving of over 30%, at the cost of a reduction in IMEP, and therefore performance, of almost 15%. Results depicted in Figure 6, are listed in the following table, Table 5.

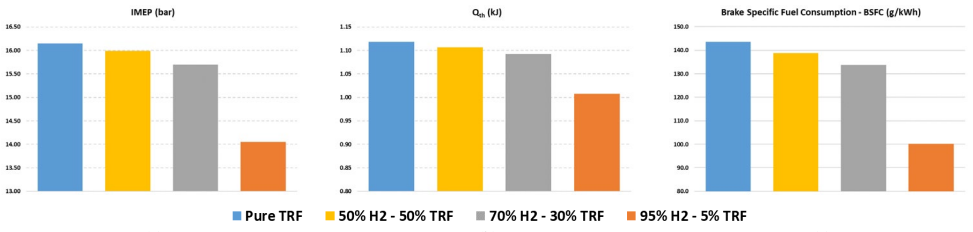

(a) (b) (c)

Figure 6 – IMEP, Q_{th}, and BSFC for the different blends on equal inlet conditions.

Table 5 - IMEP, Q_{th}, and BSFC values reached with the different blends under the same inlet conditions.

	Spark Time (CA deg)	IMEP (bar)	Q_{th} (kJ)	BSFC (g/kWh)	BSFC Reduction
Pure TRF	690.0	16.150	1.1181	143.5819	/
50% H2 - 50% TRF	696.5	15.989	1.1065	138.7446	3.37%
70% H2 - 30% TRF	701.5	15.697	1.0922	133.8383	6.79%
95% H2 - 5% TRF	713.4	14.053	1.0076	100.1743	30.23%

To evaluate the potential BSFC gain on equal IMEP, inlet conditions are adjusted to counterbalance the lower density of H2. Thus, intake pressure is progressively increased in the H2-doped simulations. The inlet temperature, as well as the overall ϕ, are kept unaltered. With these updated inlet settings, all the simulations share almost equal Q_{th}, within a range of +0.09 – +1.32%. For the sake of clarity, all the values are listed in Table 6. SA is again adjusted to meet nearly equal phasing of 50% MFB. A further increase in SA with respect to the previous cases is needed. As depicted in Figure 7, all the simulations reach 50% of MFB within a range of -0.50 and +0.50 CAdeg.

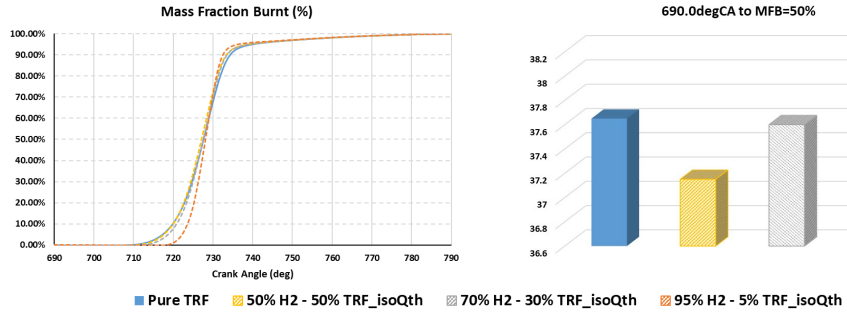

(a) (b)

Figure 7 – MFB plot for the different tested blends on equal Q_{th}.

The increased Q_{th}, as expected, leads to progressive increase of pressure peak for increasing H2 content. Now, the available energy is the same for the different simulations, and the increase of H2 directly impacts on the power output of the engine. In-cylinder pressure traces, as well as the apparent heat release ones (AHRR), are shown in Figure 8.

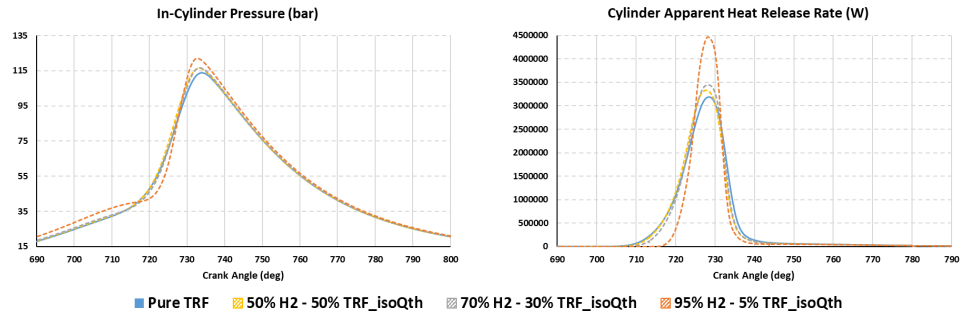

(a) (b)

Figure 8 – In-cylinder pressure and AHRR traces for the different tested blends on equal Q_{th}.

Comparable IMEP values are now found, with a reduction in BSFC which reaches slightly more than 30% for the 95% H2 case with respect to the pure-TRF counterpart. Values are listed in Table 6 for the sake of clarity.

Table 6 - IMEP, Q_{th}, and BSFC values reached with the different tested blends, by introducing almost the same Q_{th} in the combustion chamber.

	Spark Time (CA deg)	IMEP (bar)	Q_{th} (kJ)	BSFC (g/kWh)	BSFC Reduction
Pure TRF	690.0	16.150	1.1181	143.5819	/
50% H2 - 50% TRF isoQ_{th}	697.0	16.171	1.1192	138.7609	3.36%
70% H2 - 30% TRF isoQ_{th}	701.9	16.122	1.1214	133.7946	6.82%
95% H2 - 5% TRF isoQ_{th}	713.7	15.841	1.1331	99.9388	30.40%

Results from this preliminary analysis seem to suggest that doping the fuel with H2 and operating the engine on equal available energy, a gain in performance can be achieved. Even more promising, a remarkable reduction in tailpipe emissions due to the reduction of carbon-content of the fuel is found. In fact, progressively lower CO, CO_2 and NO masses are found in the cylinder at EVO, as reported in Table 7.

Table 7 – Tailpipe emissions for the different blendson equal Q_{th}.

	CO mass (mg)	CO Reduction	CO2 mass (mg)	CO2 Reduction	NO mass (mg)	NO Reduction
Pure TRF	1.55	/	83.99	/	1.24	/
50% H2 - 50% TRF isoQ_{th}	1.49	3.43%	79.67	5.13%	1.22	2.08%
70% H2 - 30% TRF isoQ_{th}	1.44	6.61%	74.60	11.18%	1.18	4.92%
95% H2 - 5% TRF isoQ_{th}	0.98	36.40%	41.39	50.71%	0.96	23.19%

In particular, the 95% mol case shows a massive reduction of around 23% in NO, 36% in CO and 50 % in CO2 mass.

5 Summary/Conclusions

Four different TRF-H2 blends are formulated, and their combustion behavior is studied using a 3D-CFD. To this aim, an ad-hoc LFS correlation is developed, following a previously presented methodology. The different blends are compared both on equal inlet conditions and on equal energy availability. On equal inlet conditions, a higher mole fraction of H2 in the fuel results in a moderate improvement in BSFC up to a cap fraction, above which the loss in performance becomes critical. Better results are achieved by changing the inlet conditions to reach equal available energy Q_{th} in the combustion chamber. With an average intake pressure increase of nearly 11%, the power-output can be kept equal to the original gasoline-only case. Such performance is achieved with a reduction of almost 32% in fuel mass per engine cycle and with a drop of CO, CO_2, and NO massed at EVO. While not addressed in this preliminary study, the addition of H2 is expected to speed up combustion through the increase of LFS. This may help reducing combustion CoV and sporadic events such as misfire and knock.
The activity will be extended to cover pure H2 fueling as well as to move from premixed inlet charge to a more challenging direct H2 injection scenario.

Reference

1 E. Commission. Secretariat-General ***EUR-Lex - 52019DC0640***, (2019).
2 E. Parliament. Council of the European Union ***EUR-Lex - 32009L0028***, (2009).

3 E. Commission. Directorate-General for Climate Action ***EUR-Lex - 52017PC0676***, (2017).
4 E. Parliament. Council of the European Union ***EUR-Lex - 32018L2001***, (2018).
5 L. Tao, E. C. D. Tan, R. McCormick, M. Zhang, A. Aden, X. He, and B. T. Zigler. Biofuels, Bioproducts and Biorefining ***8***, **no. 1** 30-48 (2013). https://doi.org/10.1002/bbb.1431
6 L. G. Pereira, M. O. S. Dias, A. P. Mariano, R. Maciel Filho, and A. Bonomi. Applied Energy ***160*** 120-31 (2015). https://doi.org/10.1016/j.apenergy.2015.09.063
7 A. Irimescu, S. S. Merola, S. Di Iorio, and B. M. Vaglieco. Fuel ***216*** 121-41 (2018). https://doi.org/10.1016/j.fuel.2017.11.116
8 S. Di Iorio, F. Catapano, P. Sementa, B. M. Vaglieco, S. Florio, E. Rebesco, P. Scorletti, and D. Terna. *SAE Technical Paper Series*, SAE International, (2014). https://doi.org/10.4271/2014-32-0038
9 S. M. Sarathy, A. Farooq, and G. T. Kalghatgi. Progress in Energy and Combustion Science ***65*** 67-108 (2018). https://doi.org/10.1016/j.pecs.2017.09.004
10 S. Verhelst, and T. Wallner. Progress in Energy and Combustion Science ***35***, **no. 6** 490-527 (2009). https://doi.org/10.1016/j.pecs.2009.08.001
11 M. Shelef, and C. A. Kukkonen. Progress in Energy and Combustion Science ***20***, **no. 2** 139-48 (1994). https://doi.org/10.1016/0360-1285(94)90008-6
12 A. d'Adamo, M. Riccardi, M. Borghi, and S. Fontanesi. Processes ***9***, **no. 3** 564 (2021). https://doi.org/10.3390/pr9030564
13 M. Riccardi, A. d'Adamo, A. Vaini, M. Romagnoli, M. Borghi, and S. Fontanesi. E3S Web Conf. ***197*** 05004 (2020). https://doi.org/10.1051/e3sconf/202019705004
14 A. D'Adamo, M. Riccardi, C. Locci, M. Romagnoli, and S. Fontanesi. *SAE Technical Paper Series*, SAE International, (2020). https://doi.org/10.4271/2020-24-0016
15 S. D. Zambalov, I. A. Yakovlev, and A. S. Maznoy. Energy Conversion and Management ***220*** 113097 (2020). https://doi.org/10.1016/j.enconman.2020.113097
16 S. Verhelst, P. Maesschalck, N. Rombaut, and R. Sierens. International Journal of Hydrogen Energy ***34***, **no. 5** 2504-10 (2009). https://doi.org/10.1016/j.ijhydene.2009.01.009
17 E. Ranzi, A. Frassoldati, R. Grana, A. Cuoci, T. Faravelli, A. P. Kelley, and C. K. Law. Progress in Energy and Combustion Science ***38***, **no. 4** 468-501 (2012). https://doi.org/10.1016/j.pecs.2012.03.004
18 E. Ranzi, C. Cavallotti, A. Cuoci, A. Frassoldati, M. Pelucchi, and T. Faravelli. Combustion and Flame ***162***, **no. 5** 1679-91 (2015). https://doi.org/10.1016/j.combustflame.2014.11.030
19 M. Del Pecchia, S. Breda, A. D'Adamo, S. Fontanesi, A. Irimescu, and S. Merola. SAE International Journal of Engines ***11***, **no. 6** 715-41 (2018). https://doi.org/10.4271/2018-01-0174
20 M. Del Pecchia, and S. Fontanesi. Fuel ***279*** 118337 (2020). https://doi.org/10.1016/j.fuel.2020.118337
21 M. Del Pecchia, V. Pessina, F. Berni, A. d'Adamo, and S. Fontanesi. Fuel ***264*** 116741 (2020). https://doi.org/10.1016/j.fuel.2019.116741

22 V. K. Krastev, A. d'Adamo, F. Berni, and S. Fontanesi. International Journal of Engine Research ***21***, **no. 4** 632-48 (2019). https://doi.org/10.1177/1468087419851905
23 C. Iacovano, A. d'Adamo, S. Fontanesi, G. Di Ilio, and V. K. Krastev. International Journal of Engine Research ***0***, **no. 0** 1468087420931712 (2020). https://doi.org/10.1177/1468087420931712
24 V. K. Krastev, G. Di Ilio, C. Iacovano, A. d'Adamo, and S. Fontanesi. E3S Web Conf. ***197*** 06021 (2020). https://doi.org/10.1051/e3sconf/202019706021
25 F. Rulli, A. Barbato, S. Fontanesi, and A. d'Adamo. International Journal of Engine Research ***22***, **no. 5** 1440-56 (2020). https://doi.org/10.1177/1468087419896469
26 F. Rulli, S. Fontanesi, A. d'Adamo, and F. Berni. International Journal of Engine Research ***22***, **no. 1** 222-42 (2019). https://doi.org/10.1177/1468087419836178
27 C. Iacovano, Y. Zeng, M. Anbarasu, S. Fontanesi, and A. D'Adamo. *SAE Technical Paper Series*, SAE International, (2021). https://doi.org/10.4271/2021-01-0399
28 Y. Shekhawat, D. C. Haworth, A. d'Adamo, F. Berni, S. Fontanesi, P. Schiffmann, D. L. Reuss, and V. Sick. Oil & Gas Science and Technology - Rev. IFP Energies nouvelles ***72***, **no. 5** 32 (2017). https://doi.org/10.2516/ogst/2017028
29 S. Fontanesi, S. Paltrinieri, A. Tiberi, and A. D'Adamo. *SAE Technical Paper Series*, SAE International, (2013). https://doi.org/10.4271/2013-01-1080
30 S. Breda, A. D'Adamo, S. Fontanesi, N. Giovannoni, F. Testa, A. Irimescu, S. Merola, C. Tornatore, and G. Valentino. SAE International Journal of Engines ***9***, **no. 1** 641-56 (2016). https://doi.org/10.4271/2016-01-0601
31 A. D'Adamo, S. Breda, S. Iaccarino, F. Berni, S. Fontanesi, B. Zardin, M. Borghi, A. Irimescu, and S. Merola. SAE International Journal of Engines ***10***, **no. 3** 722-39 (2017). https://doi.org/10.4271/2017-01-0551
32 S. Fontanesi, G. Cicalese, A. d'Adamo, and G. Cantore. Energy Procedia ***45*** 769-78 (2014). https://doi.org/10.1016/j.egypro.2014.01.082
33 A. d'Adamo, C. Iacovano, and S. Fontanesi. Applied Energy ***280*** 115949 (2020). https://doi.org/10.1016/j.apenergy.2020.115949
34 F. Berni, and S. Fontanesi. Applied Thermal Engineering ***174*** 115320 (2020). https://doi.org/10.1016/j.applthermaleng.2020.115320
35 F. Berni, G. Cicalese, M. Borghi, and S. Fontanesi. Applied Thermal Engineering ***190*** 116838 (2021). https://doi.org/10.1016/j.applthermaleng.2021.116838
36 F. Berni, S. Fontanesi, G. Cicalese, and A. D'Adamo. SAE International Journal of Commercial Vehicles ***10***, **no. 2** 547-61 (2017). https://doi.org/10.4271/2017-01-0569
37 S. Fontanesi, G. Cicalese, A. D'Adamo, and G. Pivetti. *SAE Technical Paper Series*, SAE International, (2011). https://doi.org/10.4271/2011-24-0132
38 M. Metghalchi, and J. C. Keck. Combustion and Flame ***48***, **no. 2** 191-210 (1982). https://doi.org/10.1016/0010-2180(82)90127-4
39 S. Breda, A. D'Adamo, S. Fontanesi, F. D'Orrico, A. Irimescu, S. Merola, and N. Giovannoni. SAE International Journal of Fuels and Lubricants ***10***, **no. 1** 32-55 (2017). https://doi.org/10.4271/2017-01-0546

40 M. Del Pecchia, S. Fontanesi, J. Prager, C. Kralj, and H. Lehtiniemi. Applied Energy ***280*** 115909 (2020). https://doi.org/10.1016/j.apenergy.2020.115909

Definitions/Abbreviations

AfTDC	After Firing Top Dead Center
AHRR	Apparent Heat Release
BDC	Bottom Dead Center
BSFC	Brake Specific Fuel Consumption
CA	Crank Angle
CFD	Computational Fluid Dynamics
CoV	Coefficient of Variation
CO	Carbon Monoxide
CO2	Carbon Dioxide
CV	Control Volume
DES	Detached Eddy Simulation
DI	Direct-Injection
DISI	Direct-Injection Spark-Ignition
EGR	Exhaust Gas Recirculation
Eq	Equation
EU	European Union
EVO	Exhaust Valve Opening
GDI	Gasoline Direct Injection
GHG	Anthropogenic Greenhouse Gas
HC	Hydrocarbon
H2	Hydrogen
H2ICE	Hydrogen-Fueled Internal Combustion Engine
ICE	Internal Combustion Engine
IMEP	Indicated Mean Effective Pressure
LES	Large Eddy Simulation
LFS	Laminar Flame Speed
LHV	Lower Heating Value
MARS	Monotone Advection and Reconstruction Scheme
MFB	Mass Fraction Burnt
NOx	Nitrogen Oxides
PFI	Port Fuel Injection
PISO	Pressure Implicit with Splitting of Operator
PM	Particulate Matter
Qth	Theroretical Energy
RANS	Reynolds Average Navier Stokes
RED	Renewable Energy Directive
RNG	Renormalization Group
SI	Spark-Ignition

SO2	Sulphur Dioxide
TDC	Top Dead Center
TRF	Toluene Reference Fuel
ULG95	“Average Gasoline”, EN228 Specification